J Mater Sci (2009) 44:1676–1686
DOI 10.1007/s10853-008-3221-x

Characterization of alumina interfaces in TBC systems

B. A. Pint · K. L. More

Received: 25 September 2008 / Accepted: 22 December 2008 / Published online: 4 February 2009

Abstract Interfacial segregants in thermally grown α-Al_2O_3 scales formed during high temperature exposure of thermal barrier coating systems reflect the oxygen-active dopants present in the bond coating and substrate, such as Y and Hf. These dopants diffuse outward and segregate to the substrate-alumina interface and the alumina grain boundaries. Related studies suggest that these segregants affect the growth and mechanical properties of the alumina-scale; however, the characterization of segregation in alumina formed on coated superalloy systems has been limited. Segregation examples evaluated using analytical transmission electron microscopy are given from traditional Pt-modified aluminide coatings and newer Pt diffusion coatings. Model systems are used to illustrate that grain boundary segregants on the columnar alumina boundaries are not because of the reverse diffusion of cations from the Y_2O_3-stabilized ZrO_2 top coating, and that interstitial elements in the substrate likely affect the outward flux of cation dopants. The dynamic nature of this segregation and oxygen-potential gradient-driven diffusion is discussed in light of observations of substrate dopant and interstitial contents affecting coating performance.

Introduction

A thermal barrier coating (TBC) system, typically used to protect Ni-base superalloys in the hot section of turbine engines, is composed of an oxidation-resistant metallic bond coating and a low thermal conductivity ceramic top coating [1–6]. Deposition and repair of TBCs is a very profitable business and, therefore, many details are proprietary. Until the past decade, there was relatively little published information about TBC performance and there is still very little in the literature about current developments. For example, few papers discuss the latest $Gd_2Zr_2O_7$ (GZO) coatings [7, 8] that have lower thermal conductivity than the more widely evaluated Y_2O_3-stabilized ZrO_2 (YSZ) coatings. Perhaps more importantly than thermal conductivity, GZO coatings also are attractive as an outer layer on YSZ because of their resistance to attack from liquid-phase silicates (the so-called CMAS for calcia-magnesia-alumino-silicates) in the engine due to ingestion of particulates such as sand [9, 10].

Since the earliest TBC performance models [2, 5], there has been a focus on the "weak link" of the TBC system—the thermally grown alumina scale that forms at the interface between the bond coating and the almost oxygen-transparent, ceramic YSZ top coating. Particularly, for YSZ deposited by electron-beam physical vapor deposition (EB-PVD) on bond coatings with a relatively flat external surface, most failures are observed at the metal–alumina interface [11]. A thermally grown α-Al_2O_3 layer is common to virtually all high-temperature TBC systems because of its slow growth rate and thermodynamic stability, particularly in the presence of water vapor in the gas from combustion [12]. On conventional high-temperature alloys and NiCoCrAlY-type bond coatings, adhesion of alumina scales is commonly improved by minor additions of oxygen-active or reactive element (RE) dopants such as Y or Hf [13–16]. These dopants are commonly found segregated to α-Al_2O_3 grain boundaries and the metal–scale interface. The segregation is thought to (1) change the scale growth mechanism thereby lowering the parabolic rate constant by up to an

B. A. Pint (✉) · K. L. More
Materials Science and Technology Division, Oak Ridge National Laboratory, Oak Ridge, TN 37831-6156, USA
e-mail: pintba@ornl.gov

order of magnitude [16] and (2) improve scale adhesion by segregating to the metal-scale interface [15] thereby preventing the detrimental segregation of indigenous sulfur [17–19]. Dopant segregation on scale grain boundaries has been observed in Pt-modified diffusion aluminide coatings where a RE was not added to the coating but diffused from the substrate [20]. The perceived effect of RE dopants on oxidation behavior also has changed because it was observed that RE grain boundary segregants improved the creep strength of bulk aluminas [21, 22]. Recently, it also was demonstrated that a RE-doped alumina scale had a lower creep rate than an undoped scale [23].

The purpose of this article is to provide examples of interfacial segregation in scales formed on bond coatings and model systems and discuss the driving force for and role of interfacial segregation in TBC systems, particularly in light of recent studies [24, 25] that have found critical effects of substrate chemistry on TBC performance but have not investigated segregation or other microchemistry phenomena in those systems.

Experimental procedure

The superalloy substrates were commercially fabricated and compositions determined by inductively coupled plasma analysis and glow discharge mass spectroscopy. Compositions are given in atomic percent. The model substrates used in this study were cast or extruded at Oak Ridge National Laboratory (ORNL). Fabrication details of the oxide-dispersed FeCrAl alloy are available elsewhere [26]. The coatings were fabricated commercially or by standard methods described elsewhere [27, 28]. Isothermal and cyclic oxidation exposures were performed in dry, flowing O_2. The cyclic tests consisted of insertion for 1 h followed by 10 min cooling between cycles. For this study, the alumina interfaces were primarily characterized using a Hitachi model HF-2000 transmission electron microscope (TEM) operated at 200 kV as well as a Philips model CM-200 scanning transmission electron microscope (STEM) also operated at 200 kV and equipped with an energy dispersive X-ray (EDX) analyzer. Cross-sectional TEM specimens were prepared using focused ion beam (FIB) thinning [29]. A W layer was applied to protect the outer surface of the reaction product from ion beam damage during thinning.

Results

Segregation in bond coatings

Some examples are given of segregation in the scale formed on actual bond coatings. Figure 1 shows the alumina scale formed beneath a commercial EB-PVD YSZ layer with a Pt-modified aluminide bond coating applied to an alloy N5 (2nd generation single crystal Ni-14Al-8Cr-7Co-2Ta-2 W-1Re-1Mo-0.05Hf superalloy) substrate after oxidation for 20 cycles at 1130 °C. The scale has the typical columnar α-Al_2O_3 microstructure [15, 16, 30] with an overlying fine-grained mixed Al_2O_3-ZrO_2 zone [31, 32] between the alumina and the YSZ top coating. Figure 1b shows an STEM/EDX Hf map near the metal–oxide interface highlighting Hf segregation on the alumina grain boundary. The N5 substrate beneath the coating contained only 0.05%Hf. The Hf segregation at the substrate–alumina interface is not apparent in this map because of the low level of Hf present in this system. Similar examples of Hf segregation can be found elsewhere [20, 33]. However, no

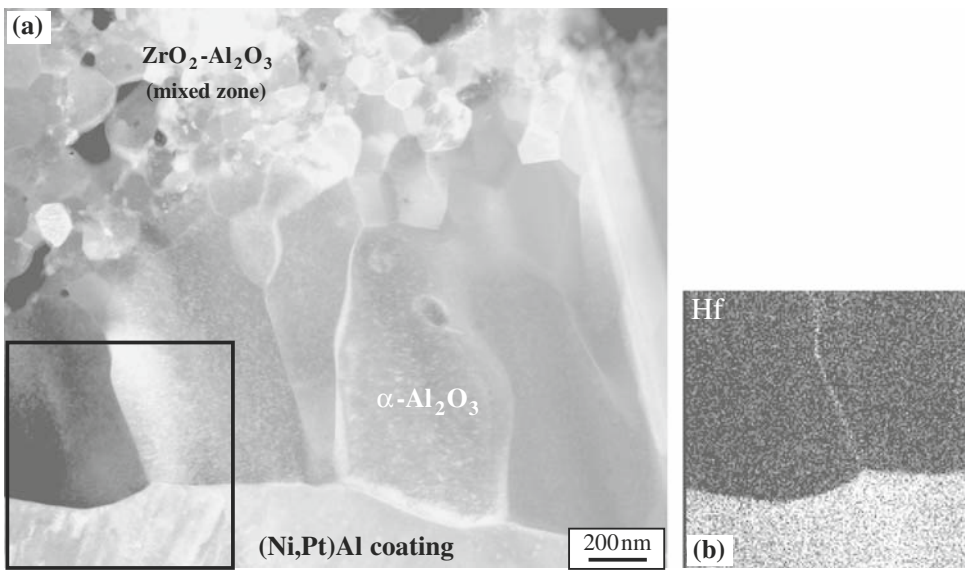

Fig. 1 **a** TEM dark field image of the alumina scale formed after 20 cycles at 1130 °C on a commercial TBC on an N5 substrate consisting of a Pt-modified aluminide bond coating and an EB-PVD YSZ top coat. **b** Hf map from the box in (**a**) showing grain boundary segregation

Hf segregation was detected in a simple (i.e., no Pt) diffusion aluminide (NiAl) coating on the same N5 substrate with 0.05Hf [20]. Studies of model alloys have suggested a synergism between Hf and Pt where Pt lowers the Hf activity thereby increasing the Hf chemical potential gradient in the substrate and increasing the driving force for incorporation of Hf into the coating [34]. For Pt aluminide coatings on superalloys without Hf (i.e., no Hf in the system), no cation segregation on the alumina grain boundaries was reported [35]. However, in that study, both TEM and Auger electron spectroscopy (AES) were used to measure S segregation at the metal–scale interface.

Figure 2 shows both Hf and Y segregation with a Pt-diffusion coating [27, 36–39]. This coating initially consisted of a 7-μm thick layer of Pt that was diffused for 2 h at 1175 °C into an N5 substrate with Y and no ceramic top coating was present [40]. The specimen was oxidized for 1,000 1 h cycles at 1150 °C to form a relatively thick oxide, compared to Fig. 1. In this case, both Hf and Y were observed as grain boundary segregants with a much lower level of Ta segregation. This N5 substrate was shown to contain 0.011% Y and 0.043% Hf but 2.1%Ta using inductively coupled plasma analysis. Thus, the amount of segregation is not proportional to the substrate concentration.

Segregation of Y also would be expected in MCrAlY-type (M = Ni, Co) bond coatings where Y is present in the 0.2–0.5% range. However, several TEM studies of this class of coating have focused on the bond coating chemistry [41], oxide pegs [42, 43], or the mixed Al_2O_3-ZrO_2 zone [32, 44, 45] but have not characterized segregation to the grain boundaries in the columnar alumina portion of the scale. Similar to MCrAlY coatings, uncoated second generation superalloys (e.g., alloys N5, 1484, and CMSX4) form a columnar α-Al_2O_3 scale underneath an initial or transient Ni-rich mixed oxide layer [16, 46, 47]. Figure 3 demonstrates that dopants in the superalloy (0.003Y, 0.003Zr, 0.054Hf, 2.11Ta) become segregants on the grain boundaries. However, as in Fig. 2, the amount of segregation was not proportional to the substrate dopant content, particularly for Ta, where segregation is not distinct in Fig. 3e. (The elemental maps in Fig. 3 are not quantitative but the Hf segregation is clearly stronger than the other elements.) Earlier work on a similar uncoated N5 substrate clearly showed Ta segregation on α-Al_2O_3 grain boundaries; however, in that case the oxidation exposure was 100 h at 1200 °C [16]. While Ta has been observed to segregate to alumina grain boundaries, it is not considered a strongly beneficial dopant and alone it did not produce the same benefit as Y or Hf [26].

Segregation in model systems

While examples from real coating systems and superalloys illustrate that segregation is not a laboratory or model alloy curiosity, TBC systems are generally so complex that it is difficult to conduct controlled experiments to elucidate mechanisms. For example, a model NiCrAlYHf alloy was made to study the segregation expected on the alumina grain boundaries in a commercial co-doped (both Y and Hf) NiCoCrAlY bond coating [14], and it was determined that there was not a different level of Y or Hf grain boundary segregation compared with a single dopant model alloy (i.e., NiCrAlY) [47].

Simple ternary Ni–Al–Hf alloys are easier to characterize for segregation because other elements are not present that may have peaks which overlap in the X-ray energy spectra. Figure 4a shows the scale formed on Ni-34Al + 0.06Hf after 2 h at 1200 °C. The martensitic structure in this two-phase ($\gamma' + \beta'$) alloy can be seen in the substrate. Because of the 34% Al content, this alloy initially formed an outer $NiAl_2O_4$ layer with an underlying alumina layer. One Ni-rich grain is apparent in the area mapped in Fig. 4b. At

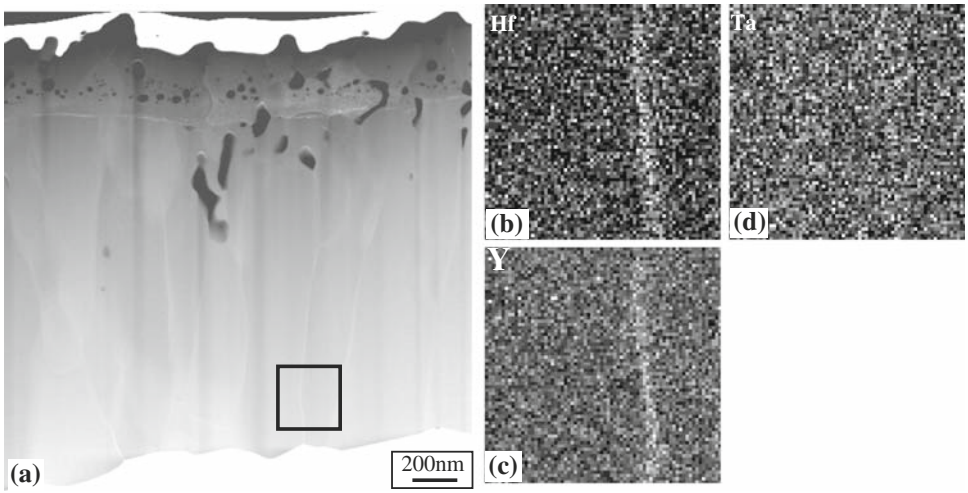

Fig. 2 **a** TEM bright field image of the alumina scale formed after 1000 1 h cycles at 1150 °C on a Pt-diffusion-coated N5 + Y substrate. The box in **a** was analyzed by STEM/EDX and elemental maps for **b** Hf, **c** Y, and **d** Ta are shown

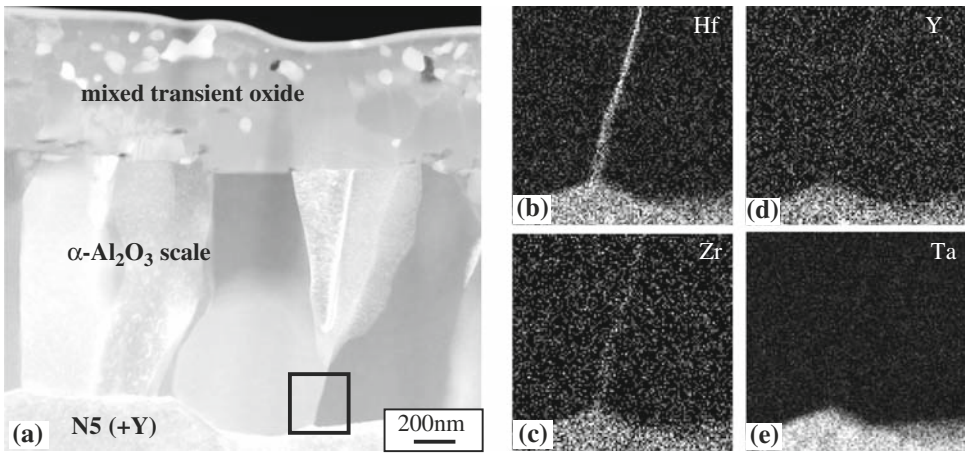

Fig. 3 **a** STEM annular dark field image of the alumina scale formed on an uncoated N5 + Y substrate after 100, 1 h cycles at 1100 °C. The box in **a** was analyzed by STEM/EDX and elemental maps for **b** Hf, **c** Zr, **d** Y, and **e** Ta are shown to illustrate grain boundary segregation on a grain boundary near the metal–scale interface

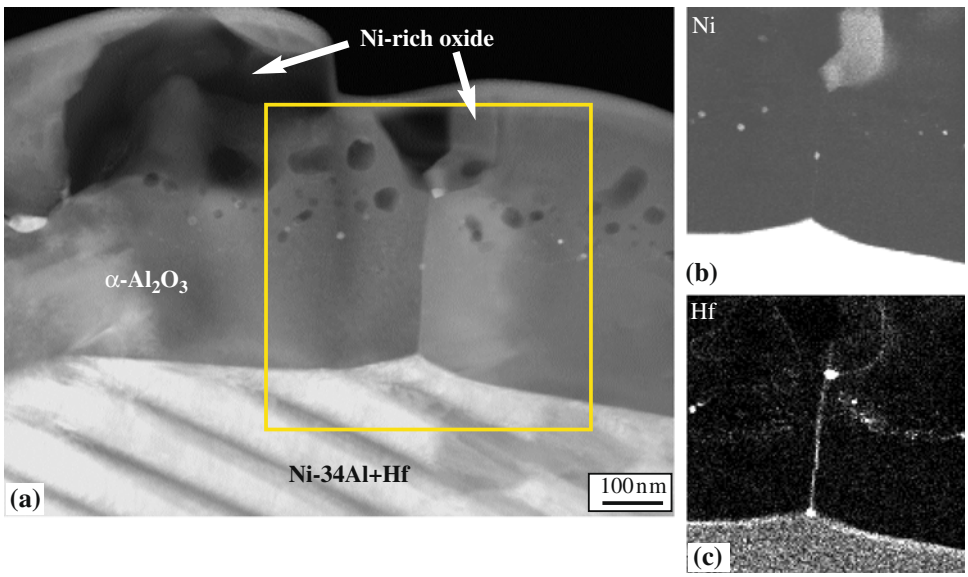

Fig. 4 **a** STEM annular dark field image of the alumina scale formed on martensitic Ni–34.4Al–0.056Hf after 2 h at 1200 °C. The box in **a** was analyzed by STEM/EDX and elemental maps for **b** Ni and **c** Hf are shown

this oxidation temperature and Hf content, the Hf map clearly shows segregation on both the oxide grain boundaries and the metal–scale interface (Fig. 4c). Hf-rich oxide particles also are present in the alumina layer as well as a few Ni-rich particles. The outer portion of the alumina layer also contains numerous voids. Previous studies have associated these voids and particles with the phase transformation of the initially formed, metastable cubic phase (e.g., θ-Al_2O_3) to the stable α phase [46, 48]. Cubic aluminas have a higher volume and cation solubility than α-Al_2O_3 resulting in voids and second-phase precipitates on transformation.

Model alloys also can help explain some of the composition effects observed in superalloys. Recent work showed an effect of different Hf and C substrate levels on Pt-modified aluminide bond coating performance [24]. Previous work had shown an effect of the Hf/C ratio on scale adhesion of model Ni-50Al alloys [49, 50], similar to the effect of dopant–impurity ratios suggested by Sigler and Smialek [51, 52]. Figure 5 shows two regions from Ni-50.1Al-0.048Hf (Hf/C = 1.4) showing the variability in scale microstructure, likely due to substrate orientation [53–55]. Figure 5a is a classic example of a thicker scale near the oxide grain boundary where transport is faster and thinner scale in the center of a large alumina grain. The ridge formed above the grain boundary corresponds to the alumina ridges observed at the gas interface (Fig. 6a). Figure 5b shows another region where the grains are smaller, the ridge spacing is closer, and an interfacial void has formed. Hafnium grain boundary segregation in this specimen has been reported previously [56, 57].

Increasing the C content in Hf-doped NiAl (49.8%Al–0.051%Hf) and thereby lowering Hf/C to 0.9 resulted in several changes. In Fig. 6b, the oxide ridges at the gas interface increased in height and width, and the spacing decreased. In the TEM cross section in Fig. 7a, the average scale grain width was smaller and the gas interface ridge structure was not apparent in this area. Instead, there was a layer of fine grains at the gas interface. Hafnium was weakly detected as a segregant to the alumina grain

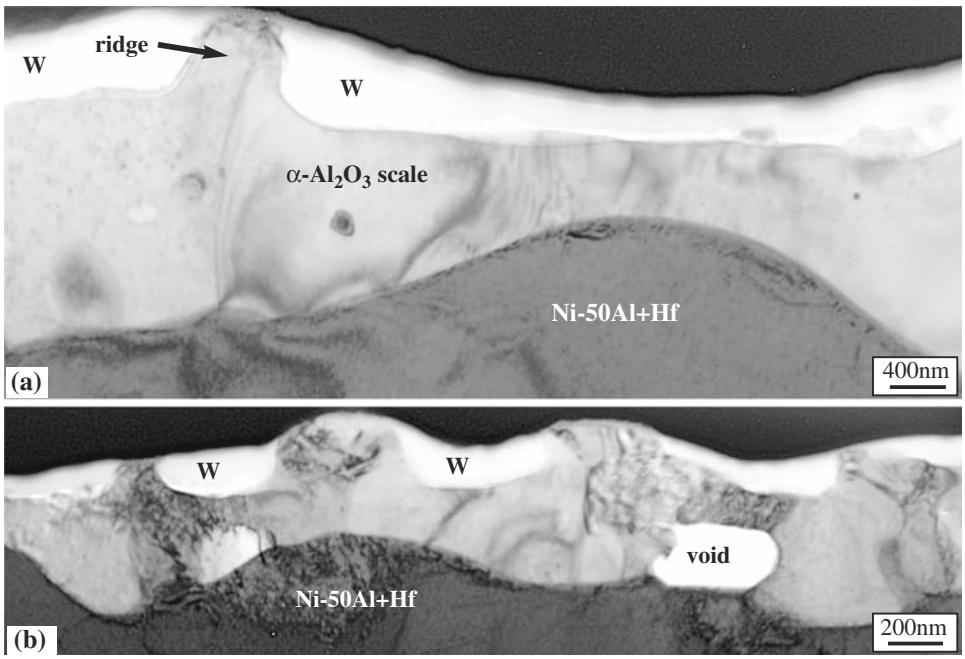

Fig. 5 TEM bright field images of the scale formed on Ni-50Al + 0.05Hf (Hf/C = 1.4) after 2 h at 1200 °C. Two locations showing different scale microstructures formed

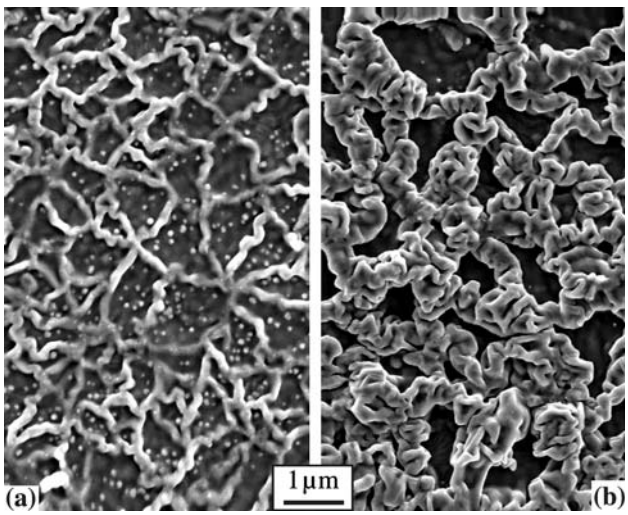

Fig. 6 SEM secondary electron plan view images of the α-Al_2O_3 scale formed on NiAl + Hf alloys after 2 h at 1200 °C **a** Hf/C = 1.4 and **b** Hf/C = 0.9

boundaries (Fig. 7b). In other regions, voids were observed at the metal–scale interface similar to Fig. 5b. However, at a longer oxidation times, the scale formed on the NiAl with Hf/C = 1.4 remained flat and adherent (Fig. 8a). In contrast, the scale formed on the lower Hf/C ratio NiAl after the same exposure showed undulations above separations between oxide and metal which were associated with large interfacial voids. The degradation in scale adhesion due to the addition of C has been attributed to a Hf–C interaction where C reduced the flux of Hf into the scale, presumably because of the formation of HfC precipitates in the metal [49, 50]. A similar effect on alumina spallation behavior was found with Zr and C in Fe-40Al [58]. When Hf/C > 1, more Hf remains in solution and is more easily incorporated into the growing scale. To confirm this hypothesis, more in-depth analytical TEM work is in progress to quantify the amount of segregation as a function of the Hf/C ratio in the substrate.

Another issue that was addressed by a model system was that of segregant source. It could be argued that the YSZ top coating contains Y, Zr, and Hf (as a naturally occurring ZrO_2 impurity). In the presence of a YSZ top coating, these elements could potentially dope the alumina scale grain boundaries. However, the dynamic segregation theory (DST) to explain the role of RE dopants suggests that the large oxygen potential gradient (OPG) across the scale prevents the backward diffusion of oxygen-active RE dopants [15]. (A role of the OPG was originally suggested by Cotell, Yurek, and coworkers to explain why ion implanted Y did not reverse diffuse in Cr_2O_3 scales [59, 60]) To test the OPG-based theory, a model substrate *without* Y, Zr, or Hf was selected, La_2O_3-dispersed FeCrAl (Fe–20Cr–9Al–1.1O–0.022La) [26]. A coupon of this alloy was coated with 125 μm of EB-PVD YSZ. It was oxidized isothermally for 200 h at 1200 °C to grow a thick α-Al_2O_3 scale. Figure 9a–c show a grain boundary analysis in the columnar section of the scale. In this area, no Y, Hf, or Zr (Fig. 9c) segregation was detected but La ions (Fig. 9b) were detected as segregants. In the outer, fine-grained mixed scale, both La and Zr (Fig. 9d and e) could be detected on the alumina grain boundaries. However, this outer layer may have grown by some outward transport that would intermix the scale and the YSZ coating providing a source of Zr ions to segregate.

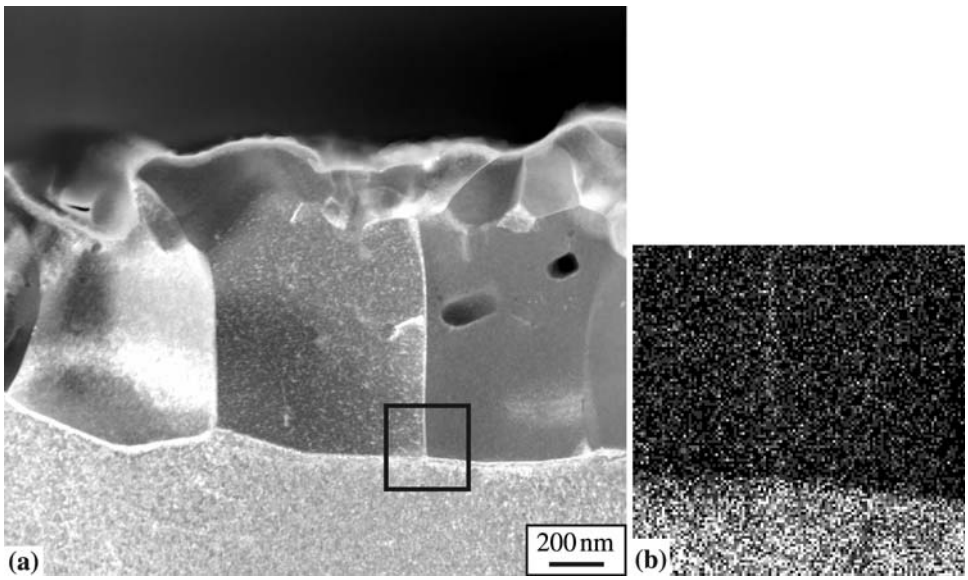

Fig. 7 **a** STEM annular dark field image of the alumina scale formed after 2 h at 1200 °C on Ni–49.8Al–0.051Hf (Hf/C = 0.9). The box in (**a**) was analyzed by STEM/EDX and the elemental map for Hf is shown in (**b**)

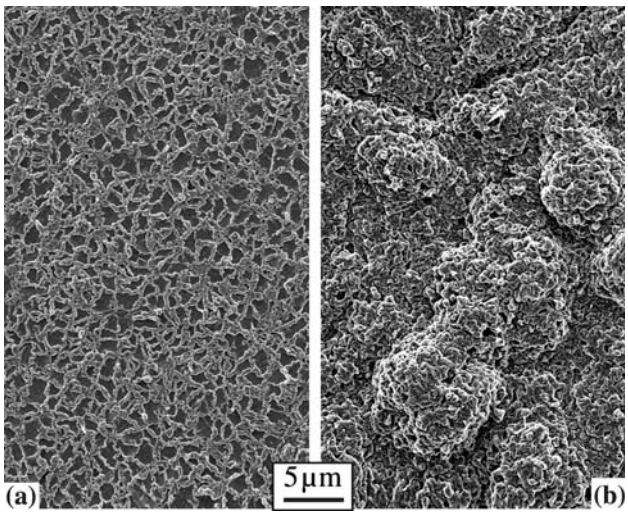

Fig. 8 SEM secondary electron plan view images of the α-Al_2O_3 scale formed on NiAl + Hf alloys after 100 h at 1200 °C **a** Hf/C = 1.4 and **b** Hf/C = 0.9

A general conclusion from model systems is that it is difficult to quantify the amount of segregation on scale interfaces and compare between systems because, as in bulk α-Al_2O_3, the amount of segregation is a function of the dopant type and exposure temperature [61]. A further complication in the analysis of scales is that the amount of segregation is dependent on the location (depth) in the scale and the time of exposure. For example, Fig. 10 shows an example of Y and Zr segregation in the alumina scale formed on Y_2O_3-dispersed Ni_3Al (22.1%Al–0.06Zr–0.56Y) beneath an outer Ni-rich oxide [62]. Similar variations have been observed in other systems [63]. Segregation on grain boundaries also can change as a function of oxidation time [64]. As the dopant diffuses outward into the scale, the boundaries can become supersaturated with segregant near the gas interface and a dopant-rich oxide particle (e.g., $Y_3Al_5O_{12}$ or HfO_2) can nucleate at or near the gas interface. After nucleation, the amount of segregant is reduced as the nearby particle becomes a sink for further segregants that diffuse to the gas interface [64]. Dopant-rich oxide particles also form due to internal oxidation and become incorporated into the inward growing alumina scale [65]. Therefore, there can be dopant-rich oxides throughout the scale. Deeper in the scale, these oxides likely act as sources for segregant ions (rather than as sinks when near the gas interface), similar to RE-rich oxide dispersions in alloys being a source for dopant ions in the scale.

Discussion

These examples of segregation at alumina interfaces have attempted to illustrate that interfacial segregation is a ubiquitous observation in RE-doped alumina scales, both in model systems and commercially made TBC's, and that there is a significant level of complexity to this phenomenon. Interfacial S segregation was not mentioned in these observations because RE segregation appears to preclude S segregation which is typically found in undoped systems, particularly at the metal–scale interface [19, 35, 66, 67]. A review of S segregation observations was recently published [68]. While dopant grain boundary segregation was first hypothesized 30 years ago [69], it took several years before TEM/EDX observations began confirming dopant segregation on scale grain boundaries [70, 71]. Another decade passed before interfacial segregation at both scale grain boundaries, and the metal–scale interface was placed in the more complete DST context of dopant ions not as

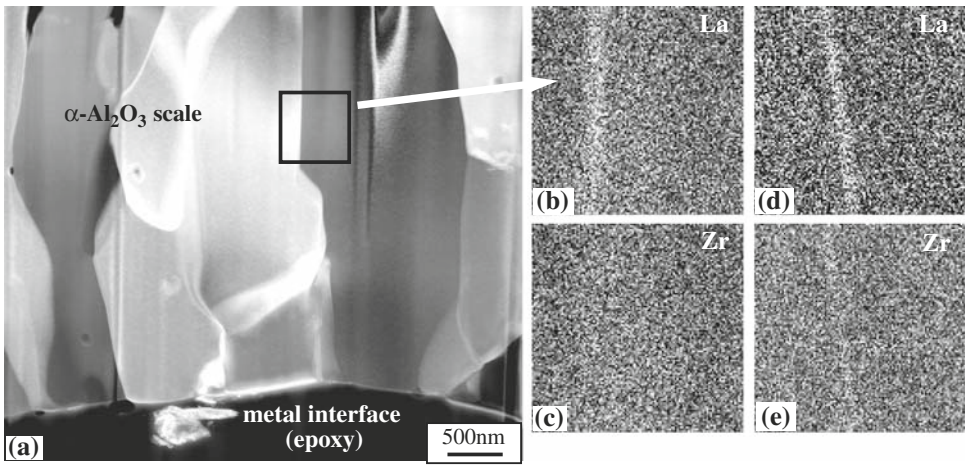

Fig. 9 Alumina scale formed on EB-PVD YSZ-coated La_2O_3-dispersed FeCrAl after 200 h at 1200 °C (**a**) shows the columnar section of the scale and maps (**b**) and (**c**) indicate La but not Zr segregation in box in (**a**). On an alumina grain boundary in the Al_2O_3–YSZ mixed zone, both (**d**) La and (**e**) Zr segregated

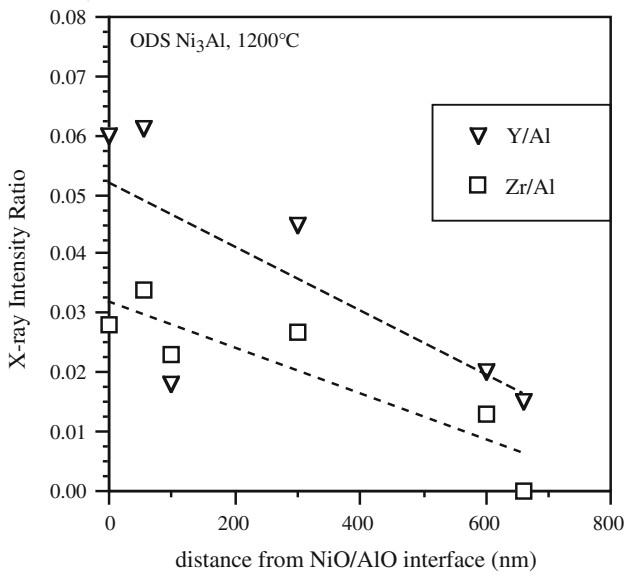

Fig. 10 Plot of grain boundary segregation as a function of depth in the α-Al_2O_3 scale for ODS Ni_3Al after oxidation for 40 h at 1200 °C [after data from 62]

stagnant segregants (as in bulk ceramics) but as diffusing species driven by the OPG to move from the substrate to the scale–gas interface [15]. This theory clearly explained why RE-rich coatings and RE ion implantation have a limited effect [72], because they cannot provide a continuous flux of RE dopant to the metal–alumina interface and alumina grain boundaries. Since the proposal of DST, no alternative mechanism for the RE effect or contradictory experimental evidence has been published.

The basic aspects of interfacial segregation in thermally grown alumina are similar to grain boundary segregation in bulk α-Al_2O_3. Based on McLean [73], segregation can be related [61] to the misfit strain energy such that for segregants with an ionic radius, r_{seg}, similar to the ionic radius of Al, r_{Al}:

$$\ln\left(C_{gb}/C_{lat}\right) \sim \left(r_{seg} - r_{Al}/r_{Al}\right)^2 \quad (1)$$

where C_{gb} and C_{lat} are the concentrations of the segregant on the grain boundary and lattice, respectively. Li and Kingery [61] matched their bulk alumina grain boundary segregation data to this relationship. The relationship could not be applied to Zr and La because they were not detected by STEM/EDX in the lattice (i.e., $C_{lat} \sim 0$) after annealing at 1775 °C. A C_{lat} value of 0.0009 was determined for Y after annealing at 1575 °C [61]. The importance of annealing temperature is that higher temperatures should decrease the amount of segregation because the strain energy driving force should decrease as the dopant is more easily accommodated in the lattice. (This argument assumes a relatively rapid cooling rate that fixes the dopant distribution.) Thus, C_{gb}/C_{lat} was 27 for Y at 1575 °C and 5.6 at 1800 °C. Cation valence did not strongly affect segregation except for Ti^{+4} where a space–charge effect was hypothesized [61].

Comparing segregation data for bulk and thermally grown alumina is difficult because of this temperature effect on segregation. To make an appropriate comparison, Zr segregation levels in alumina scales [64] were compared to Zr segregation on Al_2O_3–Al_2O_3 grain boundaries found in Al_2O_3–ZrO_2 bulk ceramics as a function of annealing temperature (Fig. 11). All of the specimens were air cooled after withdrawing from the furnace. The segregation values (in this case the peak Zr/Al intensity ratio at the interface as $C_{lat} \sim 0$) decreased with annealing temperature for the bulk Al_2O_3–ZrO_2 specimens and were consistent with the Zr segregation level reported by Li and Kingery [61]. The segregation levels in the thermally grown scales did not follow the same temperature trend. The reason is attributed to a critical difference between bulk and thermally grown alumina. The bulk specimens follow equilibrium segregation behavior in alumina with a fixed dopant content. In the scale, the grain boundaries are not just segregation sites to

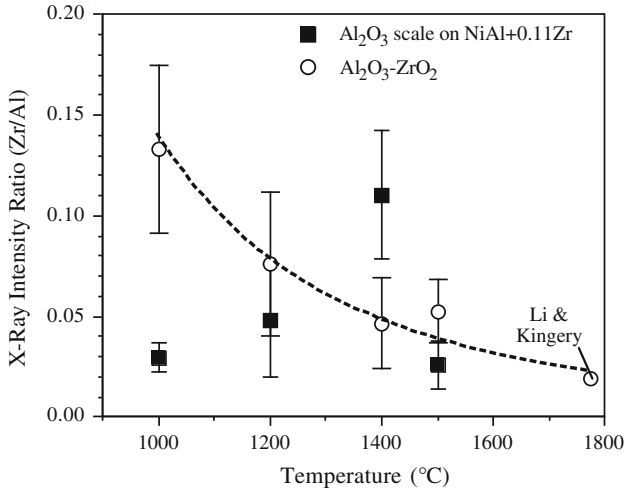

Fig. 11 Segregation of Zr to alumina–alumina grain boundaries as a function of annealing for bulk ceramics* or oxidation temperature for scales [64]. Results from Zr-doped Al_2O_3 also are included [61]. Bars show standard deviation of ~6 measurements. *Data from unpublished work of B. A. Pint and K. B. Alexander, Oak Ridge, TN (1997)

relieve strain energy but also a diffusion path. An additional driving force besides strain is affecting segregation in scales: the OPG. Oxygen-active RE dopants can lower their free energy by diffusing from the metal into the oxide all the way to the highest oxygen potential at the gas interface. Thus, the oxidation temperature not only affects how much segregant is present on the scale grain boundaries because of strain energy but also affects the amount of dopant in the scale due to the outward dopant flux into the scale. This is particularly important at lower oxidation temperatures. At 1500 °C, the outward flux of dopant is sufficiently high that ZrO_2 particles nucleate and grow at the gas interface (e.g., Fig. 12a), their volume increasing with oxidation time [64, 74]. In this near-equilibrium case, the Zr segregation is similar to that formed in a bulk ceramic. In contrast, for oxidation at 1000 °C the Zr segregation value was low (Fig. 11) because only a small flux of Zr was present in the scale after 50 h, with few ZrO_2 particles. A measurement after 5,000 h at 1,000 °C would likely find a higher level of segregation as more Zr diffused into the scale. The opposite behavior was found after a 1 h exposure at 1400 °C where the Zr/Al measurement was extremely high because the grain boundaries were supersaturated at the point where nucleation of ZrO_2 particles occurred at the gas interface of the scale [64]. A longer exposure at 1400 °C would likely yield a lower amount of segregation, closer to the equilibrium segregation value. Thus, the reason for segregation in scales is not unrelated to strain energy, that driving force moves the dopants to the boundaries rather than the lattice. However, a second driving force, the OPG, is involved which affects the dopant concentration in the scale and makes the segregation time dependent—a dynamic aspect to the segregation. By selecting appropriate oxidation times at each temperature, the scale segregation values in Fig. 11 would likely move closer to the equilibrium behavior.

As to which alloy dopants segregate, the list is very similar as those that segregate in bulk alumina [61]. However, dopants that are less oxygen active than Al, in particular Mn and V, were not found as grain boundary segregants when added as a dispersion (MnO and VN) to FeCrAl [26]. It was argued that those elements with an oxygen affinity lower than Al were not incorporated into the oxide and were not affected by the OPG. Therefore, they did not segregate to scale grain boundaries as they were observed to do in bulk alumina [61].

Beyond the issue of which elements segregate is the more relevant question of which elements produce the RE benefit on alumina growth and adhesion, i.e., which dopants are *effective* segregants. Again, the previous study on oxide-dispersed FeCrAl [26] provides the best indication that a number of small cations (e.g., Mg, Ti, Ta, Nb) segregate but do not confer as significant a benefit as larger cations (i.e., high r_{seg}). Therefore, simply segregating to the grain

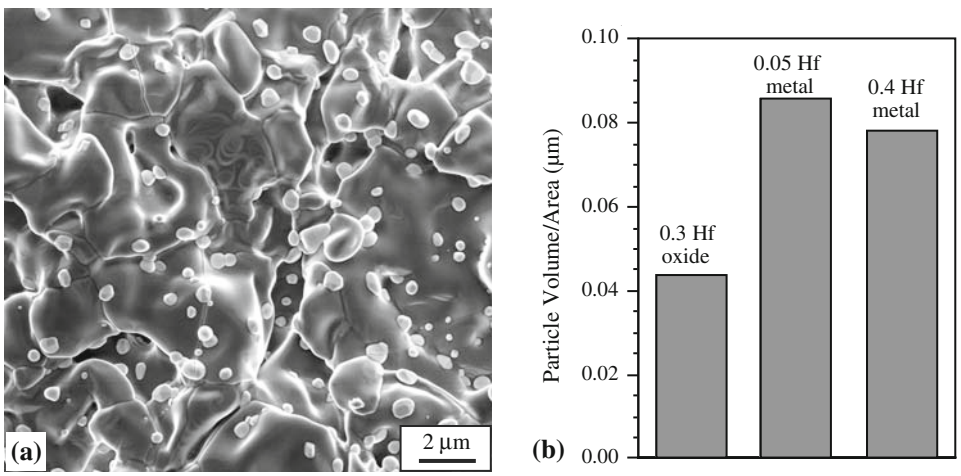

Fig. 12 **a** SEM secondary electron plan view image of the gas interface of the alumina scale formed on HfO_2-dispersed NiAl after 4 h at 1500 °C showing the HfO_2 particles that nucleate and grow. **b** Quantification of the HfO_2 particle volume formed after 4 h at 1500 °C on three different Hf-doped NiAl alloys

boundaries is not sufficient to produce the beneficial effect. Based on the examples and literature cited above, the most well-known effective dopants are all large ions: Y, Hf, Zr, and La. Hafnium is the most recent addition to that list with work emanating from the screening studies of Doychak [75] and the coating studies on Hf-containing superalloys of Streiff and coworkers [76]. The relative benefit of RE dopants on alumina scale growth or adhesion does not scale with ion size as was observed for RE dopants on the growth rate of the Cr_2O_3 scale formed on oxide-dispersed Ni–25Cr [77]. However, the relative benefit of similar dopants on lowering the creep rate of bulk alumina is not simply a function of ion size but a more complex relationship with the atomic bonding at the grain boundary [22]. Thus, cation size is not the sole criterion for determining effectiveness but does give some indication.

The examples above also introduced the effectiveness of co-doping or using multiple RE dopants to improve oxidation behavior [14, 47, 78, 79]. There is a similar analogy in bulk ceramics with combinations of elements such as Nd and Zr having an additional beneficial effect on creep strength [80]. In alumina scales, the co-doping benefit does not appear to be related to the amount of segregation [47]. Rather, the alloy co-doping strategy for oxidation resistance allows replacing Y in the alloy with Hf and/or Zr. The significance of this replacement is that Y is virtually insoluble in Fe- and Ni-based alloys and tends to form Y-rich precipitates on the grain boundaries. (This low solubility is a key reason for the thermal stability, i.e., low coarsening rate, of Y-containing oxide dispersion strengthened alloys [26].) These Y-rich metallic particles tend to internally oxidize forming Y–Al oxides such as $Y_3Al_5O_{12}$ that allow more rapid O transport than does α-Al_2O_3, thereby increasing the rate of oxidation and promoting deeper internal oxidation [78]. In single crystal superalloys, Y additions also attack the casting molds and are only tolerated at low (5–50 ppm) levels [81]. At these low levels, Y is ineffective as a single dopant. Therefore, pairing Y with a more soluble dopant is an effective strategy. Additions of Hf and Zr alone are not as effective as when combined with Y [78]. A unique aspect of Y may be its interaction with S [18, 19]. Sulfides of Hf and Zr are not as stable as Y sulfides [51]. This may explain why the Y/S ratio is a critical factor [51, 52, 78], although the importance of this relationship also may be related to the potential for segregation of both elements at the metal–scale interface [15] rather than a gettering mechanism [18].

There is a general issue about the role of interstitials (most importantly S, but also C, P, etc.) and their interaction with dopants that has been recognized for the last 20 years [51]. The recent work showing the effect of Hf and C superalloy content on coating performance [24] illustrated that dopant-interstitial effects need to be broadly considered beyond just S and the gettering mechanism. One aspect of the results for model Ni–Al–Hf–C substrates presented in Figs. 6, 7, 8 is that varying the Hf/C ratio in these materials did not eliminate the Hf benefit but did reduce it. This suggests that a more sophisticated argument than gettering—Hf tied up as HfC—is needed. Previous work comparing Hf and HfO_2 additions in NiAl [74] clearly demonstrated that when Hf was added as HfO_2, there was a reduction in the HfO_2 particle volume at the gas interface that formed due to the outward diffusion of Hf through the scale during oxidation for 4 h at 1500 °C, Fig. 12. (The other interesting result was that the HfO_2 volume was not strongly affected by the amount of Hf metal added to the alloy, Fig. 12b.) As mentioned previously, a similar effect may occur when more HfC forms due to higher C levels in the substrate, i.e., lower Hf/C. The C addition likely reduced the Hf outward flux and thereby makes the Hf addition less effective. A similar interaction likely occurs for low levels of Y and S. In this dynamic system, a reduction in mobility is critical. Therefore, awareness of the dopant-interstitial ratios is another critical factor, particularly when minimizing the RE content of the system.

Considering the current understanding of dopant and interstitial effects on alumina scale adhesion, one of the unresolved issues is the observed effect of small RE dopant additions [81] and very low S levels in the superalloy on the performance of TBC lifetimes particularly with MCrAlY bond coatings. In the case of diffusion aluminide coatings, there is no RE added to the system other than that present in the superalloy. Even with Pt in an aluminide coating, the RE benefit appears to be much more significant than the Pt benefit [16]. The addition of Pt only affects adhesion and does not slow the alumina growth rate. Therefore, scale growth and adhesion on aluminide coatings should be more affected by superalloy composition as has been observed in several studies [20, 24, 25, 38, 82, 83]. However, in the case of MCrAlY coatings, which generally contain 0.05–0.5%Y, there should be a larger quantity of Y in the coating than S or dopant atoms in the substrate. Modifications of CMSX4 reportedly had a *combined* Y + La content of 5 ppmw [81]. Even with a large coating:substrate ratio of 1:50 (e.g., 40-μm coating on a 2-mm thick turbine foil substrate) there should be more Y in the coating than in most superalloy substrates, and enough Y to counteract a few ppm S in the substrate. However, the limited experimental evidence in the literature suggests that substrate composition has dramatic effects on TBC lifetime with MCrAlY bond coatings [81–83]. The dynamic aspect and role of interstitials needs to be considered in this case, as shown schematically in Fig. 13. If the bond coating is losing Y because of its outward flux into the scale ($J_{RE(bc)}$) and internal oxidation of Y (i.e., oxide peg formation [42, 43]) also reduces Y mobility, the coating may effectively run out of Y during service [84].

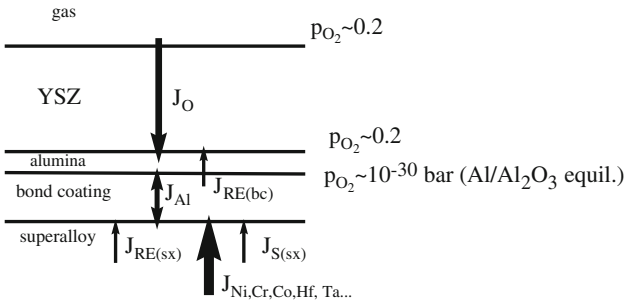

Fig. 13 Schematic of diffusion fluxes in a generic TBC system. Interdiffusion occurs between the superalloy substrate and the metallic bond coating. Oxygen readily diffuses through the yttria-stabilized ZrO_2 (YSZ) top coating. The oxidation reaction to form alumina primarily involves the inward transport of O with a minor contribution of Al outward transport. Equilibrium at the alumina–substrate interface requires a very low partial pressure of O_2, and thus a very high oxygen potential gradient which is the driving force for diffusion of oxygen-active or -reactive elements (RE) from the substrate

At this point, S diffusing from the substrate through the coating ($J_{S(SX)}$) could affect the alumina adhesion but a flux of RE dopant from the substrate ($J_{RE(SX)}$) could continue to dope the coating and supply dopant to the alumina scale. The test of this hypothesis will be to look for a unique superalloy dopant such as La in the alumina scale when an MCrAlY coating was used. This hypothesis of dopant depletion was developed to explain the effect of MCrAlY coating thickness [84] and also the effect of substrate thickness on the oxidation behavior of alumina-forming alloys [85].

A better understanding of dopant effects and quantifying the amount of segregation is needed not only to improve the performance of current TBC technology but also to assist in the development of the next generation of alloys and coatings. Development efforts for next generation alloys, whether they be higher performance or lower cost, need guidance on the optimization of minor alloying additions. Perhaps a performance breakthrough will occur because of a different dopant element or a new combination of dopants. These efforts may be assisted by computational methods which are now being used to study segregation and interfaces [86, 87]. However, these models need to be based on the correct driving forces in order to provide relevant information. The driving force due to the OPG is critical in thermally grown scales but difficult to quantify because there are few experiments that isolate the OPG role [88–90]. The OPG present in solid oxide fuel cells between the air and fuel sides may affect long-term performance of functional multi-cation oxides in that system [90].

In conclusion, this review has focused on the segregation phenomenon and its implications to TBC systems. Details critical to future segregation studies have not been addressed, such as the quantification method of the interfacial segregation, the potential errors associated with the measurement, and possible distortions due to the specimen-thinning process. These issues will need to be addressed in subsequent studies to create a better understanding of the role of interfacial segregation in TBC systems.

Summary

A number of examples were shown of STEM/EDX segregation observations in thermally grown α-Al_2O_3 scales both from commercial and laboratory-made TBC bond coatings and from model bond coating alloys. Several key points are emphasized:

1. Segregation of dopant ions is found in all systems doped with a reactive element such as Y, Zr, and Hf.
2. The oxygen potential gradient across the scale represents a driving force not found in bulk alumina. Segregants in alumina scales are not statically located on the grain boundaries, but diffuse outward during oxidation and are prevented from diffusing back toward the alloy because of the dopant–oxygen chemical potential gradient.
3. Examples were shown to illustrate that the segregation in alumina scales is affected by time, temperature, and interstitial content.
4. The dynamic nature of the outward dopant flux and the finite dopant content in the TBC system needs to be considered in coating lifetime models.
5. Segregation in TBC systems needs to be further quantified as a function of system composition, time, and temperature and this information needs to be incorporated into computational modeling of thermally grown alumina systems.

Acknowledgements The authors would like to thank C. Leyens, DLR, Köln, Germany for coating the FeCrAl substrate; K. Cooley, L. D. Chitwood, G. Garner, K. S. Reeves, J. L. Moser, H. Longmire, and D. Coffey at ORNL for assistance with the experimental work; I. G. Wright and M. P. Brady at ORNL; P. Y. Hou at LBL for manuscript comments. This research was sponsored by the U.S. Department of Energy, Office of Coal and Power R&D, Office of Fossil Energy (R. Dennis—program manager) under contract DE-AC05-00OR22725 with UT-Battelle, LLC.

References

1. Stecura S (1977) Am Ceram Soc Bull 56:1082
2. Miller RA (1984) J Am Ceram Soc 67:517
3. Strangman TE (1985) Thin Solid Films 127:93
4. Goward GW (1986) Mater Sci Technol 2:194
5. Cruse TA, Stewart SE, Ortiz M (1988) J Eng Gas Turbines Power 110:610
6. Goward GW (1998) Surf Coat Technol 108–109:73
7. Maloney MJ (2000) US Patent #6,117,560
8. Leckie RM, Krämer S, Rühle M, Levi CG (2005) Acta Mater 53:3281

9. Krämer S, Yang J, Levi CG (2008) J Am Ceram Soc 91:576
10. Borom MP, Johnson CA, Peluso LA (1996) Surf Coat Technol 86–87:116
11. Meier SM, Nissley DM, Sheffler KD, Cruse TA (1992) J Eng Gas Turbines Power 114:258
12. Opila EJ (2004) Mater Sci Forum 461–464:765
13. Wukusick CS, Collins JF (1964) Mater Res Stand 4:637
14. Gupta DK, Duvall DS (1984) In: Gell M et al (eds) Superalloys 1984. TMS, Warrendale, PA, p 711
15. Pint BA (1996) Oxid Met 45:1
16. Pint BA, Wright IG, Lee WY et al (1998) Mater Sci Eng A245:201
17. Ikeda Y, Nii K, Yoshihara K (1983) Trans Japan Inst Metals 24:207
18. Smeggil JG, Funkenbusch AW, Bornstein NS (1986) Met Trans 17A:923
19. Smialek JL, Jayne DT, Schaeffer JC, Murphy WH (1994) Thin Solid Films 253:285
20. Haynes JA, Pint BA, More KL et al (2002) Oxid Met 58:513
21. Cho J, Wang CM, Chan HM et al (1999) Acta Mater 47:4197
22. Yoshida H, Ikuhara Y, Sakuma T (2002) Acta Mater 50:2955
23. Veal BW, Paulikas AP, Gleeson B, Hou PY (2007) Surf Coat Technol 202:608
24. Tolpygo VK, Murphy KS, Clarke DR (2008) Acta Mater 56:489
25. Wu RT, Kawagishi K, Harada H, Reed RC (2008) Acta Mater 56:3622
26. Pint BA, Alexander KB (1998) J Electrochem Soc 145:1819
27. Zhang Y, Lee WY, Haynes JA et al (1999) Met Trans A 30A:2679
28. Zhang Y, Haynes JA, Pint BA, Wright IG (2005) Surf Coat Technol 200:1259
29. Gianuzzi LA, Stevie FA (1999) Micron 30(3):197
30. Golightly FA, Stott FH, Wood GC (1979) J Electrochem Soc 126:1035
31. Murphy KS, More KL, Lance MJ (2001) Surf Coat Technol 146–147:152
32. Braue W, Schulz U, Fritscher K et al (2005) Mater High Temp 22:393
33. Spitsberg I, More K (2006) Mater Sci Eng A417:322
34. Izumi T, Gleeson B (2006) Mater Sci Forum 522–523:221
35. Molins R, Hou PY (2006) Surf Coat Technol 201:3841
36. Bouhanek K, Adesanya OA, Stott FH et al (2001) Mater Sci Forum 369–372:615
37. Nicholls JR (2003) Mater Res Bull 28:659
38. Tawancy HM, Mohamed AI, Abbas NM et al (2003) J Mater Sci 38:3797. doi:10.1023/A:1025992502450
39. Gleeson B (2006) J Prop Power 22:375
40. Haynes JA, Pint BA, Zhang Y, Wright IG (2008) Surf Coat Technol 203:413
41. Mendis BG, Tryon B, Pollock TM, Hemker KJ (2006) Surf Coat Technol 201:3918
42. Xu T, Faulhaber S, Mercer C et al (2004) Acta Mater 52:1439
43. Mendis BG, Livi KJT, Hemker KJ (2006) Scr Mater 55:589
44. Levi CG, Sommer E, Terry SG et al (2003) J Am Ceram Soc 86:676
45. Hu M, Guo S, Tomimatsu T et al (2006) Surf Coat Technol 200:6130
46. Pint BA, More KL, Wright IG, Tortorelli PF (2000) Mater High Temp 17:165
47. Pint BA, More KL, Wright IG (2003) Mater High Temp 20:375
48. Schumann E, Schnotz G, Trumble KP, Rühle M (2005) Acta Met Mater 53:3281
49. Pint BA, Haynes JA, More KL, Wright IG (2004) In: Green KA et al (eds) Superalloys 2004. TMS, Warrendale, PA, p 597
50. Wright IG, Pint BA (2005) J Power Energy Proc IMechE 219:101
51. Sigler DR (1989) Oxid Met 32:337
52. Smialek JL, Pint BA (2001) Mater Sci Forum 369–372:459
53. Homma T, Hindam HM, Pyun Y, Smeltzer WW (1982) Oxid Met 17:223
54. Doychak J, Smialek JL, Mitchell TE (1989) Met Trans 20A:499
55. Roux JP, Brumm MW, Grabke HJ (1993) Fresenius J Anal Chem 346:265
56. Pint BA, Haynes JA, More KL et al (2000) In: Pollack TM et al (eds) Superalloys 2000. TMS, Warrendale, PA, p 629
57. Pint BA, More KL, Wright IG (2003) Oxid Met 59:257
58. Pint BA, Schneibel JH (2005) Scr Mater 52:1199
59. Cotell CM (1988) Effects of yttrium on the oxidation mechanisms of pure chromium. MIT, Cambridge, MA
60. Przybylski K, Yurek GJ (1989) Mater Sci Forum 43:1
61. Li CW, Kingery WD (1984) In: Structure and properties of MgO and Al2O3 ceramics, advances in ceramics, vol 10. Am Ceram Soc, Columbus, OH, p.368
62. Pint BA, Garratt-Reed AJ, Hobbs LW (2001) Oxid Met 56:119
63. Hiramatsu N, Stott FH (1999) Oxid Met 51:479
64. Pint BA, Garratt-Reed AJ, Hobbs LW (1998) J Am Ceram Soc 81:305
65. Naumenko D, Kochubey V, Niewolak L et al (2008) J Mater Sci 43:4550. doi:10.1007/s10853-008-2639-5
66. Hou PY, Stringer J (1992) Oxid Met 38:323
67. Hou PY (2003) J Am Ceram Soc 86:660
68. Hou PY (2008) Annu Rev Mater Res 38:275
69. Ecer GM, Meier GH (1979) Oxid Met 13:159
70. Ramanarayanan TA, Raghavan M, Petkovic-Luton R (1984) J Electrochem Soc 131:923
71. Yurek GJ, Przybylski K, Garratt-Reed AJ (1987) J Electrochem Soc 134:2643
72. Pint BA (1994) Mater Res Bull 19(10):26
73. McLean D (1957) Grain boundaries in metals. Oxford University Press, London
74. Pint BA, Alexander KB, Monteiro OR, Brown IG (1998) In: Mishin Y et al (eds) Diffusion mechanisms in crystalline materials, Symp Proc, vol 527. MRS, Pittsburgh, PA, p 497
75. Doychak J (1994) In: Westbrook JH, Fleischer RL (eds) Intermetallic compounds, vol 1: principles. Wiley, New York, p 977
76. N'Gandu Muamba JM, Streiff R, Boone DH (1987) Mater Sci Eng 88:111
77. Pint BA (2003) In: Tortorelli P F et al (ed) Proc. John Stringer symposium on high temperature corrosion, ASM International, Materials Park, OH, p 9
78. Pint BA (2003) J Am Ceram Soc 86:686
79. Naumenko D, Kochubey V, Le Coze J et al (2004) Mater Sci Forum 461–464:489
80. Li YZ, Wang CM, Chan HM et al (1999) J Am Ceram Soc 82:1497
81. Harris K, Wahl JB (2004) In: Green KA et al (eds) Superalloys 2004. TMS, Warrendale, PA, p 45
82. Kimmel J, Mutasim Z, Brentnall W (2000) J Eng Gas Turbines Power 122:393
83. Schulz U, Menzebach M, Leyens C, Yang YQ (2001) Surf Coat Technol 146–147:117
84. Toscano J, Vaßen R, Gil A et al (2006) Surf Coat Technol 201:3906
85. Quadakkers WJ, Huczkowski P, Naumenko D et al (2008) Mater Sci Forum 595–598:1111
86. Bouchet D, Lartigue-Korinek S, Molins R, Thibault J (2006) Phil Mag 86:1401
87. Milas I, Hinnemann B, Carter EA (2008) J Mater Res 23:1494
88. Schmalzried H, Laqua W, Lin PL (1979) Z Natur 34a:192
89. Petot-Ervas G, Petot C, Monceau D, Loudjani M (1992) Solid State Ionics 53–56:270
90. Kawada T, Watanabe T, Kaimai A et al (1998) Solid State Ionics 108:391